 CMES, vol.113, no.4, pp.429-441, 2017

Numerical Simulation of Coal Deformation and Gas Flow Properties Around Borehole

Yi Xue [1,2,3]

Abstract: The lack of research on the effect of diffusion on methane extraction leads to low methane concentration and low utilization. The Comsol Multiphysics software is used to solve the numerical gas and solid coupled model which considers the diffusion of coal matrix, fracture seepage, permeability evolution and coal deformation. The simulation results reveal the effect of diffusion process on methane migration. The gas diffusion rate is relatively high in the initial stage. With the increase in time, the difference between coal fractures and coal matrix blocks becomes lower and the gas diffusion rate decreases gradually. The gas seepage rate decreases significantly near the borehole and the decrease degree becomes small when it is far away from borehole. The influence of diffusion time on gas drainage rate is not obvious.

Keywords: Temperature, permeability, porosity, gas pressure, heat injection.

1 Introduction

Coal seam gas (CSG) is an important kind of clean energy, which plays an important role in the world energy structure. Underground well and ground drilling is usually used in the pre-extraction process, and the underground drainage is the main method for the actual reservoir conditions [Barenblatt, Zheltov and Kochina (1960); Cao, Zhou, Zhang et al. (2015); Xue, Gao and Liu (2015)]. However, many coal seams in the world are low-permeability coal seams, and methane stored in coal seams cannot be effectively extracted. Many technological means are adopted to increase the permeability of coal seam and achieve the efficient gas extraction. For example, hydraulic fracturing technology, carbon dioxide flooding, hot injection, and other engineering technologies have been successfully applied to enhance the extraction of coalbed methane [Douglas, Hensley and Arbogast (1991)], as shown in Figure 1.

Hot injection extraction techniques have gained great attention in recent years because of its superiority [Gray (1987); Mavor and Vaughn (1998); Hong, Koo and Park (2012);

[1] State Key Laboratory Base of Eco-Hydraulic Engineering in Arid Areas, Xi'an University of Technology, Xi'an 710048, China

[2] Institute of Geotechnical Engineering, Shaanxi Provincial Key Laboratory of Loess Mechanics and Engineering, Xi'an University of Technology, Xi'an 710048, China

[3] Corresponding author, E-mail address: xueyi@xaut.edu.cn.

High, Budianto and Oda (2016); Xue, Cao, Cai et al. (2017)]. However, the effect of temperature on coal-gas interactions in coal seam gas extraction is still not clear. Therefore, the thermal evolution characteristic evolution during the extraction of coalbed methane needs to be studied.

In this study, a gas-solid coupled model is established to describe coalbed methane migration, which combines with methane diffusion law, seepage law in coal matrix, permeability evolution model and coal seam deformation equation. The model is used to simulate the whole process of methane extraction, and the effect of diffusion on methane migration is analyzed.

Figure 1: High-pressure water jet slotting technology

2 Governing equations

2.1 Coal seam deformation

For the dual porosity media, the effective stress can be expressed as

$$\sigma_{eij} = \sigma_{ij} - \alpha p_f \delta_{ij} \tag{1}$$

where σ_{eij} is the effective stress. δ_{ij} is the Kronecker delta tensor. α is effective stress coefficients for coal fractures.

The strain-displacement relation of coal is expressed as

$$\varepsilon_{ij} = \frac{1}{2}(u_{i,j} + u_{j,i}) \tag{2}$$

The Navier-type equation is yielded as

$$Gu_{i,jj} + \frac{G}{1-2\mu} u_{j,ji} - \alpha p_{f,i} - K\alpha_T T_{,i} - K\varepsilon_{s,i} + f_i = 0 \tag{3}$$

2.2 Gas flow equation

The non-Darcy flow caused by inertial effect has a significant influence on gas reservoir performance and it can be expressed as

$$-\nabla p_f = \frac{\upsilon}{k_g}\vec{\mu} + \beta\rho_g\vec{\mu}|\vec{\mu}| \tag{4}$$

where $\vec{\mu}$ is the gas velocity vector; ρ_g is the gas density; $\beta = \frac{1.75}{\sqrt{150k_g\phi^3}}$; ϕ is the porosity of coal; k_g is the permeability of coal.

The above equation can be expressed as the following form

$$\vec{\mu} = -\frac{k_g}{(1+\frac{k_g}{\upsilon}\beta\rho_g|\vec{\mu}|)\upsilon}\nabla p_f = -\frac{k_g}{f_{qi}\upsilon}\nabla p_f \tag{5}$$

where $f_{qi}=1+\frac{k_g}{\upsilon}\beta\rho_g|\vec{\mu}|$ is a Forchheimer number.

For the porous media, the flow equilibrium equation can be expressed as

$$\frac{\partial}{\partial t}(\phi_f\rho_g) + \nabla(\rho_g\cdot\vec{\mu}) = Q_s(1-\phi_f) \tag{6}$$

where ρ_g is the density of gas; $\vec{\mu}$ is the gas velocity vector; Q_s is the gas source by injection; t is the real time; this mass content m is defined as [Izadi, Wang, Elsworth et al. (2011)]

$$m = \rho_g\phi_f + \rho_{ga}\rho_c V_{sg} \tag{7}$$

where ϕ_f is the porosity; ρ_{ga} is the gas density at standard conditions; ρ_c is the coal density; V_{sg} is the content of absorbed gas.

The gas absorption volume can be expressed as

$$V_{sg} = \frac{V_L p_f}{p_f + P_L}\exp[-\frac{c_2}{1+c_1 p_f}(T_{ar}+T-T_t)] \tag{8}$$

where VL and PL are the Langmuir volume constant and Langmuir pressure constant at temperature Tt, respectively; Tar the absolute reference temperature in the stress-free state; Tt the reference temperature for the desorption/adsorption test of gas; (Tar+T) the temperature of the coal seam; c1 the pressure coefficient; and c2 the temperature coefficient.

The sorption induced volumetric shrinkage strain ε_s is assumed as

$$\varepsilon_s = \alpha_{sg}V_{sg} \tag{9}$$

where V_{sg} is the content of absorbed gas; α_{sg} is the coefficient of sorption-induced

strain.

The ideal gas law is described as

$$\rho_g = \frac{M_g}{R(T_{ar}+T)} p \tag{10}$$

where ρ_g is the gas density; Mg is the molecular weight of the gas; T is the gas temperature; R is the universal gas constant; p_a is the standard atmospheric pressure.

Then the gas flow equation can be rewritten as

$$\frac{\rho_{ga}}{p_a}\frac{\partial(\phi_f p_f)}{\partial t} + \nabla(-\frac{k_g}{\mu}\frac{\rho_g}{f_{qi}}\nabla p_f) = Q_s(1-\phi_f) \tag{11}$$

2.3 Gas diffusion in coal matrix

The gas transport experiences three stages: flow in the fractures, gas diffusion and sorption in the matrix. Figure 1 shows a conceptual model for gas transport. The source term from the adsorption of coal matrix can be expressed as

$$Q_s = D\sigma_c(c_m - c_f) \tag{12}$$

$$\frac{\partial m_m}{\partial t} = -\frac{Mc}{\tau RT}(p_m - p_f) \tag{13}$$

where Q_s is the exchange from matrix to fractures; D is the gas diffusion coefficient; c_m is the gas concentration in matrix; c_f is the gas concentration in the fractures; σ_c is the coal matrix block shape factor.

The gas concentration in matrix and fractures can be expressed as

$$c_m = \frac{Mc}{RT} p_m \tag{14}$$

$$c_f = \frac{Mc}{RT} p_f \tag{15}$$

where Mc is the molar mass of methane; R is the universal gas constant.

The methane exchange rate is related with the current gas content and the equilibrium gas content, therefore, the following equation is introduced to calculate the exchange rate

$$\frac{\mathrm{d}m_b}{\mathrm{d}t} = -\frac{1}{\tau}(m_b - m_e) \tag{16}$$

where m_e is the equilibrium gas content under pressure p_f.

Then the diffusion equation can be expressed as

$$\frac{\partial m_m}{\partial t} = -\frac{Mc}{\tau RT}(p_m - p_f) \tag{17}$$

The effective gas permeability k_g can be expressed as [Kumar, Elsworth, Mathews et al. (2016)]

$$k_g = k_\infty(1+\frac{b}{p_f}) \tag{18}$$

where k_∞ is the intrinsic permeability, and b is the Klinkenberg coefficient, which increases with the reduction of permeability according to

$$b = \alpha_k k_\infty^{-0.36} \tag{19}$$

where α_k is the Klinkenberg effect coefficient, α_k =0.251.

2.4 Coal permeability

The general porosity model is defined as [Soofastaei, Aminossadati, Kizil et al. (2016)]

$$\Delta\phi_f = \frac{1}{K}(\beta_f - \phi_f)(\bar{\sigma} + p_f) \tag{20}$$

Then the porosity is expressed as

$$\phi_f = \alpha - (\alpha - \phi_0)\exp\{-\frac{1}{K}[(\bar{\sigma} - \bar{\sigma}_0) + (p_f - p_{f0})]\} \tag{21}$$

where subscript 0 denotes the initial state of variables.

Substituting the porosity can be rewritten as

$$\phi_f = \alpha - (\alpha - \phi_{f0})\exp\{-[(\varepsilon_V + \frac{p_f}{K_s} - \varepsilon_s - \alpha_T T) - (\varepsilon_{V0} + \frac{p_{f0}}{K_s} - \varepsilon_{s0} - \alpha_T T_0)]\} \tag{22}$$

where $S = \varepsilon_V + \frac{p_f}{K_s} - \varepsilon_s$, $S_0 = \varepsilon_{V0} + \frac{p_{f0}}{K_s} - \varepsilon_{s0}$. p_0 is the initial pressure and ϕ_0 is the initial porosity.

The permeability is correlated to the porosity according to the following exponential function

$$k_\infty = k_{\infty 0}(\phi_f / \phi_{f0})^3 \tag{23}$$

The apparent permeability in fracture system is obtained as

$$\frac{k_g}{k_{\infty 0}} = \frac{k_\infty}{k_{\infty 0}}(1+\frac{b}{p_f}) = (\frac{\phi}{\phi_0})^3(1+\frac{b}{p_f}) \tag{24}$$

2.5 Energy conservation

Neglecting the thermal-filtration effect, the total heat flux q_T is given by

$$q_T = -\lambda_M \nabla T + \rho_g C_g q_g (T_{ar} + T) \tag{25}$$

where q_T is thermal flux; ρ_s the mass density of the gas; Cg the gas specific heat constants at constant volume; q_g the Darcy velocity; $\lambda_M = (1-\phi_f)\lambda_s + \phi_f \lambda_g$, λ_M, λ_s and λ_g are the thermal conductivities of coal, solid components and gas components, respectively.

Neglecting the interconvertibility of thermal and mechanical energy, the thermal balance can be expressed as [Valliappan and Wohua (1996)]

$$\frac{\partial[(\rho C)_M (T_{ar} + T)]}{\partial t} + (T_{ar} + T) K_g \alpha_g \nabla \cdot (\frac{k_g}{\mu} \nabla p) + (T_{ar} + T) K \alpha_T \frac{\partial \varepsilon_V}{\partial t} = -\nabla \cdot q_T \tag{26}$$

where $(\rho C)_M$ is the specific heat capacity of the gas-filled solid medium, $(\rho C)_M = \phi_f (\rho_g C_g) + (1-\phi_f)(\rho_s C_s)$; ρ_s the mass density of the rock matrix; Cg and Cs the gas heat constants and solid heat constants at constant volume, respectively. α_g is the thermal expansion coefficient of the gas under constant pore pressure and stress.

The conservation of mass of the two phases yields

$$\frac{\partial[(1-\phi_f)\rho_s]}{\partial t} = 0 \tag{27}$$

$$\frac{\partial(\phi_f \rho_g)}{\partial t} = -\nabla \cdot (\rho_g q_g) \tag{28}$$

Considering $(1-\phi)\lambda_s \gg \phi\lambda_s$ and $\lambda_M \approx (1-\phi_f)\lambda_s \approx \lambda_s$, then yields

$$(\rho C)_M \frac{\partial T}{\partial t} - (T_{ar} + T) K_g \alpha_g \nabla \cdot (\frac{k_g}{\upsilon} \nabla p_f) + (T_{ar} + T) K \alpha_T \frac{\partial \varepsilon_V}{\partial t} = \lambda_M \nabla^2 T + \frac{\rho_{ga} p_f T_a C_g}{p_a (T_{ar} + T)} \frac{k_g}{\upsilon} \nabla p_f \nabla T \tag{29}$$

3 Model verification and establishment

3.1 Analytical validation

In order to verify the effectiveness of this coupled model in the calculation of gas flow in

porous media, the finite element model is applied and the numerical results are compared with the simplified analytical solutions. The one-dimensional linear steady gas flow model has a length of 20 m. A single phase gas is injected into the rock with a constant rate of gas at the inlet and gas pressure keeps constant at outlet. Assuming that the porosity of the rock remains constant, the gas will eventually reach a steady state. Equation for one-dimensional linear flow can be reduced from Eq. (6) to:

$$\frac{\partial}{\partial x}[-\frac{k_{\infty}M_g}{\upsilon RT}(p+b)\frac{\partial p}{\partial x}]=0 \tag{30}$$

The boundary conditions are

$$\begin{cases} v_g(x=0)=v_0 \\ p(x=L)=p_L \end{cases} \tag{31}$$

where v_0 is the constant injection rate at the inlet (x=0), and p_L is the constant gas pressure at the outlet (x=L). At the given boundary conditions, the one-dimensional steady-state analytic solution is given by Wu et al. [Wu, Pruess and Persoff (1998)].

$$p(x)=-b+\sqrt{b^2+p(L)^2+2bp(L)+2v_0p_a(L-x)\upsilon/k_{\infty}} \tag{32}$$

The parameters used in numerical calculation are listed in Table 1, and these parameters are also adopted in analytical solutions. This comparison shows that the numerical solutions agree well with the analytical solutions, which verifies the validity of the numerical model.

Table 1 Parameters used for one-dimensional linear steady gas flow

Parameter	Value
Young's modulus of coal (E, MPa)	2700
Young's modulus of the coal grains (E_s, MPa)	7100
Initial porosity (ϕ_0, -)	0.3
Density of coal (ρ_c, kg/m^3)	0.3
Poisson's ratio of coal (ν, -)	0.38
Initial gas permeability ($k_{\infty 0}$, m^2)	5.0×10^{-19}
Compressibility factor, (*Mc/RT*, kg/(Pa·m^{-3}))	1.18×10^{-5}
Gas dynamic viscosity (υ, N·s/m^2)	1.84×10^{-5}
Length of the rock column (*L*, m)	20

3.2 Model establishment

In order to analyze the influence of heat injection on the gas extraction, a calculation

model is established as shown in Figure 2. The length of model is 100 m and width of model is 100 m. The four boundaries are restrained by normal displacement. The zero fluxes are applied to these boundaries. The initial pressure of the coal seam is 6.2 MPa, the initial temperature of the coal seam is 293 K and the parameters in the calculation are listed in Table 2. A monitoring line is selected in diagonal line of coal mass and three monitoring points A (30 m, 30 m), B (55 m, 55 m) and C (80 m, 55 m) is used to analyze the change law of production rate, coal permeability and gas pressure.

Table 2: Property parameters used in the simulation model

Parameter	Value
Young's modulus of coal (E, MPa)	2700
Young's modulus of the coal grains (E_s, MPa)	7100
Initial porosity (ϕ_0, -)	0.01
Density of coal (ρ_c, kg/m^3)	1380
Poisson's ratio of coal (ν, -)	0.38
Initial gas permeability ($k_{\infty 0}$, m^2)	1.09×10^{-18}
Density of CH_4 at standard condition (ρ_g, kg/m^3)	0.717
Gas dynamic viscosity (υ, N·s/m^2)	1.84×10^{-5}
CH_4 Langmuir pressure constant (P_L, MPa)	1.57
CH_4 Langmuir volume constant (V_L, m^3/kg)	0.043
Specific heat capacity of gas (C_g, J/kg·K)	1.005×10^3
Specific heat capacity of coal (C_s, J/kg·K)	1.25×10^3
Pressure coefficient (c_1, MPa^{-1})	0.07
Coefficient for sorption-induced volumetric strain (α_{sg}, kg/m^3)	0.06
Volumetric thermal expansion of the solid matrix coefficient (α_T, K^{-1})	2.4×10^{-5}
Klinkenberg effect (*b*, Pa)	1.44×10^5
Temperature coefficient (c_2, MPa^{-1})	0.02
Thermal conductivity of coal (λ_s, J/m·s·K)	0.2

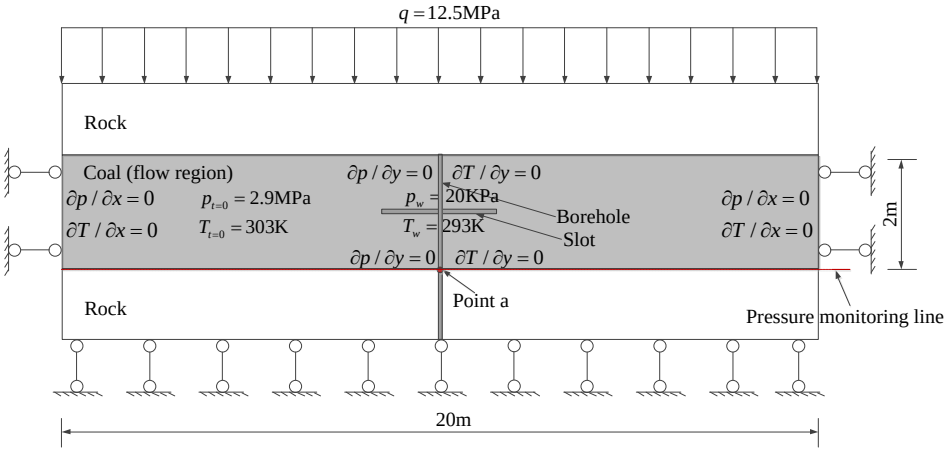

Figure 2: Computational model and the schematic diagram of heat injection well.

4 Result and discussion

4.1 Effect of diffusion on diffusion rate

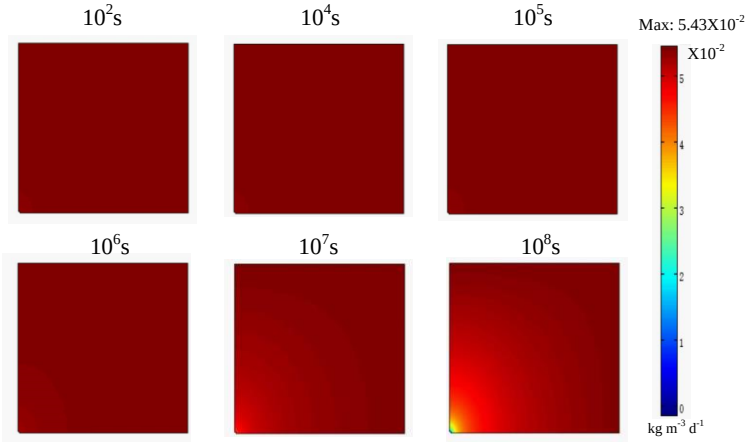

Figure 3: Gas diffusion rate distribution at different times

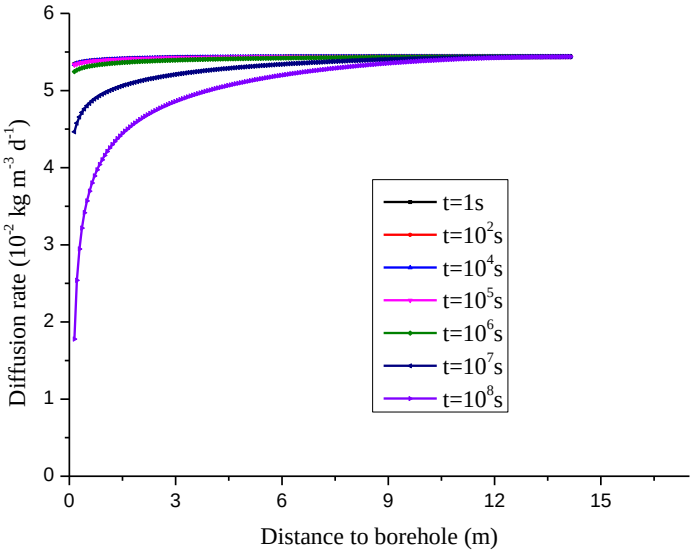

Figure 4: Gas diffusion rate along the diagonal line

Figure 3 shows the gas diffusion rate distribution at different times and Figure 4 shows the gas diffusion rate along the diagonal line. The effect of diffusion on gas extraction can be seen from these figures. In the initial gas extraction process, the gas in the fractures can flow to the borehole quickly under the influence of pressure gradient. Therefore, the gas diffusion rate is relatively high in the initial stage. With the increase in time, the difference between coal fractures and coal matrix blocks becomes lower and the gas diffusion rate decreases gradually. It can be seen from the figure that the gas diffusion rate decreases significantly near the borehole and the decrease degree becomes small when it is far away from borehole.

4.2 Effect of diffusion on seepage rate

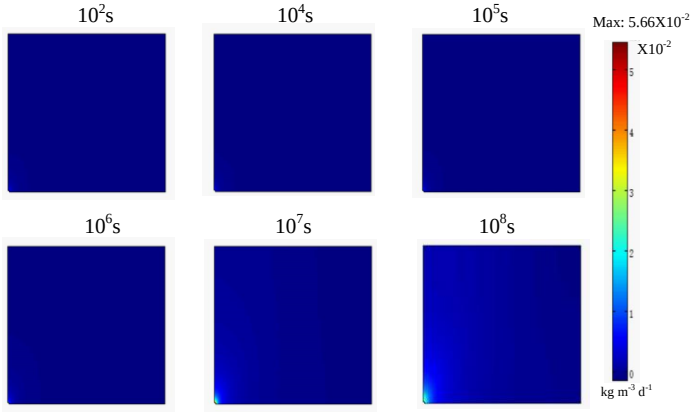

Figure 5: Gas seepage rate distribution at different times

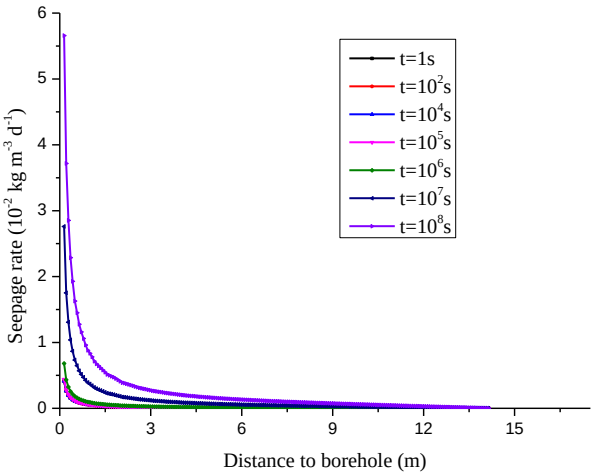

Figure 6: Gas seepage rate along the diagonal line

Figure 5 shows the gas seepage rate distribution at different times and Figure 6 shows the gas seepage rate along the diagonal line. The change law of gas seepage rate is obvious different from that of gas diffusion rate. The gas seepage rate is mainly controlled by the pressure gradient of coal fractures and the gas diffusion rate is mainly controlled by the pressure gradient of coal fractures and matrix blocks. The gas seepage rate increases gradually with the increase of time. Similar to the change law of gas diffusion rate, the gas seepage rate decreases significantly near the borehole and the decrease degree becomes small when it is far away from borehole.

4.3 Effect of diffusion on drainage rate

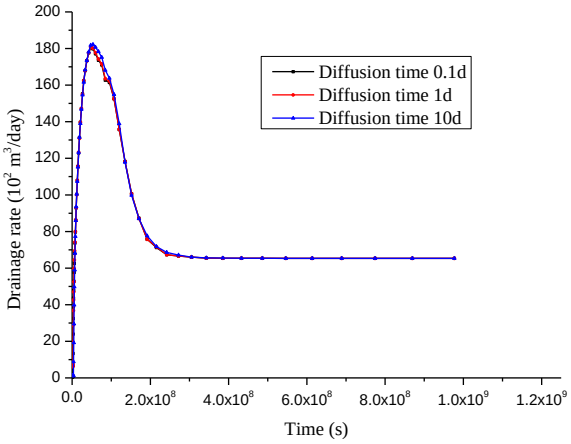

Figure 7: Gas drainage rate at different times

Figure 7 shows the gas drainage rate at different times. The influence of diffusion time on gas drainage rate can be seen from this figure. The influence of diffusion time on gas drainage rate is not obvious. When the diffusion time increases from the 0.1 d to 10 d, the gas drainage rate increases slightly. It may be caused by the fact that the gas drainage

lasts many years and the diffusion time only is some days. There is a far distance difference in the order of magnitude.

5 Conclusions

(1) In the initial gas extraction process, the gas in the fractures can flow to the borehole quickly under the influence of pressure gradient. The gas diffusion rate is relatively high in the initial stage. With the increase in time, the difference between coal fractures and coal matrix blocks becomes lower and the gas diffusion rate decreases gradually.

(2) The change law of gas seepage rate is obvious different from that of gas diffusion rate. The gas seepage rate increases gradually with the increase of time. The gas seepage rate decreases significantly near the borehole and the decrease degree becomes small when it is far away from borehole.

(3) The influence of diffusion time on gas drainage rate is not obvious. It may be caused by the fact that the gas drainage last many years and the diffusion time only is some days. There is a far distance difference in the order of magnitude.

Acknowledgments: This study is sponsored by the National Natural Science Foundation of China (no. 51679199), the Initiation Fund of Doctor's Research (no. 107-451117008), the Special Funds for Public Industry Research Projects of the Ministry of Water Resources (no. 201501034-04 and 201201053-03) and the Key Laboratory for Science and Technology Coordination & Innovation Projects of Shaanxi Province (no. 2014SZS15-Z01).

References

Barenblatt, G. I.; Zheltov, I. P.; Kochina, I. N. (1960): Basic concepts in the theory of seepage of homogeneous liquids in fissured rocks. *Journal of Applied Mathematics and Mechanics*, vol. 24, pp. 1286-1303.

Cao, Z.; Zhou, Y.; Zhang, Q.; Wang, E. (2015): Mechanical Analysis of the Coupled Gas-Solid-Thermal Model during Rock Damage. *Computers, Materials & Continua*, vol. 47, no. 3, pp. 203-215.

Douglas, J.; Hensley, J. L.; Arbogast, T. (1991): A dual-porosity model for waterflooding in naturally fractured reservoirs. *Computer Methods in Applied Mechanics and Engineering*, vol. 87, no. 2-3, pp. 157-174.

Ge, Z.; Mei, X.; Jia, Y.; Lu, Y.; Xia, W. (2014): Influence radius of slotted borehole drainage by high pressure water jet. *Journal of Mining and Safety Engineering*, vol. 31, no. 4, pp. 657-664.

Gray, I. (1987): Reservoir engineering in coal seams: Part 1-The physical process of gas storage and movement in coal seams. *SPE Reservoir Engineering*, vol. 2, no. 1, pp. 28-34.

High, A. M.; Budianto, D.; Oda, T. (2016): Computational Fluid Dynamic Analysis of Co-Firing of Palm Kernel Shell and Coal. *Energies*, vol. 9, no. 3, pp. 137.

Hong, T.; Koo, C.; Park, S. (2012): A decision support model for improving a

multi-family housing complex based on CO 2 emission from gas energy consumption. *Building and Environment*, vol. 52, pp. 142-151.

Izadi, G.; Wang, S.; Elsworth, D.; Liu, J.; Wu, Y.; Pone, D. (2011): Permeability evolution of fluid-infiltrated coal containing discrete fractures. *International Journal of Coal Geology*, vol. 85, no. 2, pp. 202-211.

Kumar, H.; Elsworth, D.; Mathews, J. P.; Marone, C. (2016): Permeability evolution in sorbing media: analogies between organic-rich shale and coal. *Geofluids*, vol. 16, no. 1, pp. 43-55.

Mavor, M. J.; Vaughn, J. E. (1998): Increasing coal absolute permeability in the San Juan Basin fruitland formation. *SPE Reservoir Evaluation & Engineering*, vol. 1, no. 1, pp. 201-206.

Soofastaei, A.; Aminossadati, S. M.; Kizil, M. S.; Knights, P. (2016): A discrete-event model to simulate the effect of truck bunching due to payload variance on cycle time, hauled mine materials and fuel consumption. *International Journal of Mining Science and Technology*, vol. 26, no. 6, pp. 995-1001.

Valliappan, S.; Wohua, Z. (1996): Numerical modelling of methane gas migration in dry coal seams. *International Journal for Numerical and Analytical Methods in Geomechanics*, vol. 20, no. 8, pp. 571-593.

Wu, Y. S.; Pruess, K.; Persoff, P. (1998): Gas flow in porous media with Klinkenberg effects. *Transp Porous Media*, vol. 32, pp. 117-137.

Xue, Y.; Gao, F.; Liu X. G. (2015): Effect of damage evolution of coal on permeability variation and analysis of gas outburst hazard with coal mining. *Natural Hazards*, vol. 79, no. 2, pp. 999-1013.

Xue, Y.; Cao, Z. Z.; Cai, C. Z.; Dang, F. N.; Hou, P. et al. (2017): A fully coupled thermo-hydro-mechanical model associated with inertia and slip effects. *Thermal Science*, vol. 21, no. S1, pp. 259-266.